Hindawi
Advances in Materials Science and Engineering
Volume 2021, Article ID 9945372, 11 pages
https://doi.org/10.1155/2021/9945372

*Research Article*

# Parameter Optimization of Graded Macadam Transitional Layer for Inverted Asphalt Pavement Based on the Mechanical Response and Strength Standard

**Chen Zhang** [1,2] **and Yong Lei** [3]

[1]*School of Energy and Architecture, Xi'an Aeronautical University, No. 259 Eastern Erhuan Road, Xi'an 710077, Shaanxi, China*
[2]*Key Laboratory for Special Area Highway Engineering of Ministry of Education, Chang'an University, Middle Section of South Erhuan Road, Xi'an 710064, Shaanxi, China*
[3]*Key Laboratory of Geological Hazards on Three Gorges Reservoir Area, China Three Gorges University, No. 8 University Road, Yichang 443002, Hubei, China*

Correspondence should be addressed to Yong Lei; leiyong@ctgu.edu.cn

Received 3 March 2021; Revised 18 April 2021; Accepted 27 May 2021; Published 8 June 2021

Academic Editor: Songtao Lv



To improve the durability of asphalt pavement with heavy traffic conditions in cold regions, the parameter optimization of graded macadam transitional layer (GMTL) for the inverted asphalt pavement based on the mechanical response and the strength standard was studied. The stress distribution laws of GMTL were studied with different loads by means of BISAR3.0. The influences of the thickness and the modulus of GMTL on the pavement stress were analyzed. The optimal thickness and the modulus range of the GMTL were determined. Combined with a self-developing real-time data acquisition and a processing system for aggregate attitude (RDAPS), the strength control standard of the GMTL was established. Finally, the performance of the optimized inverted asphalt pavement structure was verified through the MEPDG design method. The results show that the tensile stress at the bottom of the surface layer reduced by about 58%, and the shear stress in GMTL increased by about 17% when the modulus of GMTL increases from 300 MPa to 800 MPa. However, the change in modulus has no significant influence on the maximum shear stress in the asphalt surface layer and the tensile stress in the base layer bottom. When the thickness of GMTL increases from 12 cm to 20 cm, the tensile stress in the bottom of the base layer reduced by about 31%. Based on the mechanical results from simulation calculation and the technical indicator required in the field, the recommended optimal parameters of GMTL are the modulus of 700 MPa and the thickness of 18 cm. In addition, the spatial attitude angle $\Phi_N$ of wireless intelligent attitude aggregate (WIAA), the compressive strength $R_c$ standard, and the California Bearing Ratio (CBR) standard were analyzed, and the strength control standard of inverted asphalt pavement with GMTL was proposed, namely, CBR $\geq$ 354%, $R_c \geq 1.06$ MPa, and $\Phi_N \leq 3^\circ$. A significant improvement in the resistance to crack can be seen in the inverted asphalt pavement when the optimized structure was applied. Taking the 20-year service life as an example, the top-down cracks reduced by 29.3% and the bottom-up cracks reduced by 32.6% in comparison to the original structure. The recommended structural parameters of GMTL could be used to guide the construction and design of inverted asphalt pavement in cold regions.

## 1. Introduction

Under the continuous effect of heavy traffic, the traditional pavement structure design method based on the multilayer elastic theory analysis is facing a severe challenge. It is embodied in the following aspects: (1) the mechanical indexes considered are mainly tensile stress and compressive stress, which are too simple to analyze the damage mechanism of the current road under the complex traffic and climate condition. (2) The structural combination design does not adequately consider the mechanical response and material properties. These challenges lead to a terrible

decrease in the durability of asphalt pavement. Therefore, road engineers have conducted many related studies.

Karimi et al. developed an anisotropic nonlinear viscoelastic constitutive relationship that is sensitive to the tension/compression stress mode by extending Schapery's nonlinear viscoelastic model [1]. Wang et al. conducted a combined static-and-dynamics analysis to evaluate the pavement structure stress state comprehensively [2]. Lv et al. established a normalization model of fatigue characteristics for asphalt mixtures under different stress states based on the yield criterion in 3-dimensional stress states [3]. Lytton et al. addressed the measurement and modelling of the damaged properties of asphalt mixtures, including the fracture, healing, and viscoelastic deformation of the asphalt mixtures in tensile and compressive loading [4]. Si et al. built a finite element model of asphalt pavement using the software ABAQUS, which was used to analyze the thermal stress and pore water pressure in pavement structure under the condition of rainfall infiltration [5]. Behnke et al. investigated the structural long-term response of asphalt pavements (modeled as elastoplastic solid at large strains) under periodic traffic load by means of the finite element method (FEM) [6]. Assogba et al. examined the response of asphalt pavements to the combined effect of the nonlinear thermal gradient and the moving axle load by means of an advanced 3D pavement FE modelling [7]. Xie et al. analyzed the mechanical response of transverse cracks treatment in different geometrical structures under wheel load and temperature load based on the orthogonal design method [8]. All in all, various measures, such as nonlinear viscoelastic model, static-and-dynamics analysis, finite element model, and structural long-term response analysis, were used to improve the durability of the asphalt pavement. At present, each structural layer of asphalt pavement was basically designed according to the full functional requirements. Hence, it is difficult to adapt to the mechanical and functional requirements of the various structural layers of asphalt pavement [9]. For example, the upper layer mainly plays a role in the antirutting function, which means the asphalt mixture in the upper layer should have high strength. However, the resistance to cracking is also emphasized in the asphalt mixture design. In general, it is inevitably a challenge to balance the two performances mentioned above [10]. Inverted asphalt pavement (IAP) refers to a new type of asphalt pavement structure with graded gravel or asphalt stabilized gravel layer upon semirigid layer. This kind of pavement structure can effectively enhance the antirutting ability and the resistance to crack of asphalt pavement [11]. In the cold region, the main distress types of the IAP structure with graded macadam transitional layer (GMTL) are cracking in the surface layer, rutting, and shear failure in the base layer [12]. The shear failure of GMTL is essentially related to the shear deformation caused by the excessive shear stress in the structure. Therefore, the shear strength reflecting the shear deformation ability should be used as the strength control index. For the control index of shear strength of GMTL materials, scholars in China and other countries have done a lot of related researches. Lima proposed some new parameters of the Guimarães model and pointed out the necessity of granulometric distribution analysis to the stone skeleton in the granular base layer and the subbase layers [13]. Guo et al. made an analysis on the control indicators based on the damage form of the graded crushed stone (GCS) layer of the flexible asphalt pavement structure. The result showed that 10 cm thickness of asphalt surface is a turning point of change curve for the tensile stress indicator of the asphalt layer and the shear stress indicator of the graded macadam layer [14]. Han et al. adopted BISAR 3.0 program to calculate the shear stress in the graded crushed stone base. It is found that the asphalt layer should not be too thin when the thickness of the graded crushed stone base is 20 cm [15]. Xu et al. developed a plastic deformation model for the GCS base layer based on the relationship between relative deformation and plastic deformation ratio [16]. Although the proposed index can characterize the shear deformation resistance of flexible base materials, it is hard to be applied in practice because of the complex test process, the high test cost, and the inconsistent test methods.

To improve the durability of asphalt pavement with heavy traffic conditions in cold regions, the parameter optimization of GMTL for IAP based on the materials mechanical response and strength standard was conducted in this study.

## 2. Raw Materials and Experimental Methods

*2.1. Determination of Calculation Parameters for BISAR 3.0.* Based on the BISAR3.0 program, the stress, strain, and displacement of any point in the pavement structure under different layer contact conditions can be calculated, which provides data to quantitatively describe the mechanical response of the pavement structure [17]. Taking a large amount of mechanical calculation into consideration, the BISAR3.0 program was used to calculate the stress of asphalt pavement structure. The influence of the material parameters and the load changes of asphalt pavement structure on the structural stress was analyzed. During the analysis process, the pavement structure was usually regarded as a linear elastic layer system [18]. The structure and calculation parameters of the typical IAP are shown in Table 1.

The selected pavement structure type is derived from an IAP structure test section in the cold region of Hebei, China. According to the "Specifications for Design of Highway Asphalt Pavement (JTD D50-2017)," the load and calculation points are calculated using the double circular uniform vertical load [19], as shown in Figure 1.

*2.2. Selection of Strength Control Index.* According to the damage characteristics of GMTL of IAP in cold regions, the strength control index is proposed combined with California Bearing Ratio (CBR), compressive strength ($R_c$), and the spatial attitude angel of aggregate obtained from a self-developed real-time data acquisition and processing system (RDAPS). RDAPS with small volume, low cost, and high precision is developed in this study. The system consists of

Table 1: Pavement structure and parameter.

| Layer | Material type | Thickness (cm) | Modulus (MPa) | Poisson ratio |
|---|---|---|---|---|
| Top-surface | SMA-13 asphalt mastic crushed stone | 6 | 1450 | 0.25 |
| Middle-surface | AC-20 asphalt mixture | 8 | 1600 | 0.25 |
| Bottom-surface | AC-25 asphalt mixture | 10 | 1850 | 0.25 |
| Top-base | GMTL | 16 | 500 | 0.35 |
| Bottom-base | Cement stabilized macadam | 36 | 8500 | 0.25 |
| Subgrade | — | — | 40 | 0.40 |

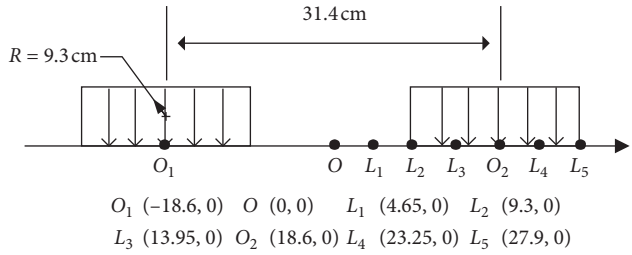


Figure 1: Cutaway drawing of load calculation point under 0.7 MPa tire ground pressure.

wireless intelligent attitude aggregate (WIAA), analysis software, and hardware equipment, as shown in Figure 2.

As seen from Figure 2(a), the WIAA with a size of 20 mm consisted of an attitude sensor, micropower supply module, and wireless transmission module (transmitter). WIAA is encapsulated by the hardened resin material using 3D printing technology. Hence, the shape of WIAA can be designed and controlled by the user. The signal stability is also acceptable due to the high mechanical strength of the WIAA shell. The micropower supply module has the function of a remote switch. The data acquisition interval can be controlled by software programming to ensure the long-term endurance of WIAA. The WIAA can output the data of the spatial attitude angle in three directions. From Figure 2(b), the software is developed by Python programming language. The aggregate attitude data can be collected, saved, and analyzed in real time. As shown in Figure 2(c), it mainly includes a wireless transmission module acting as a signal receptor, a micropower supply module acting as a control terminal, a data processing system, and a display screen. When the WIAA is implanted into GMTL, it can cooperate with graded macadam in deformation. The attitude angle of WIAA is collected and analyzed via the RDAPS, so as to quantitatively characterize the embedded state of graded macadam.

CBR can be used to characterize the load-bearing capacity and deformation resistance of materials. Moreover, the instrument used for the CBR test is convenient to operate. In case of an uneven settlement of pavement structure, $R_c$ can be used as an index to control the deformation of GMTL. During the compaction process of the graded macadam, the spatial attitude angle of WIAA would keep constant once the graded macadam is already in a dense state. In other words, the interlock skeleton was formed in the graded macadam. Therefore, CBR, $R_c$, and the attitude angle of WIAA are selected as strength design indexes of GMTL materials in this study.

*2.3. Research Process.* Firstly, the stress distribution laws of GMTL were studied with different loads by means of BISAR3.0. The influences of the thickness and the modulus of GMTL on the pavement stress were analyzed and the optimal thickness and modulus range of the GMTL was determined. Then, combined with the self-developed RDAPS, the strength control standard of the GMTL was established. Finally, the performance of the optimized IAP structure was verified through the MEPDG design method. This study has practical significance for promoting the development of IAP construction technology in cold regions and improving the durability of asphalt pavement. The research flow chart is shown in Figure 3 [20].

## 3. Results and Discussion

### *3.1. Mechanical Response Analysis*

*3.1.1. Tensile Stress and Shear Stress of Asphalt Surface Layer.* The distribution of shear stress and the tensile stress of the asphalt surface layer under 0.7 MPa load are shown in Figure 4.

Figure 4(a) shows that most of the large shear stress was seen in the range of 0 cm to 12 cm below the road surface. Among them, the maximum shear stress in the upper layer of the asphalt pavement was observed at $L_5$ point, about 4 cm from the road surface. The maximum shear stress in the middle layer appeared at $L_4$ point, 8 cm from the road surface. Therefore, $L_4$ point and $L_5$ point were chosen as the research point for the shear stress of the asphalt surface layer. Figure 4(b) shows that tensile stress occurring at the $L_1$ and the $O$ points, and the maximum tensile stress at the bottom of the asphalt layer appeared at the $O_2$ point. The $O$ and the $O_2$ points were selected as the calculation points for studying the tensile stress of the asphalt pavement surface and the asphalt layer, respectively.

*3.1.2. Shear Stress of GMTL.* For the asphalt pavement with GMTL, the tensile stress of the pavement surface is small even under heavy traffic load. The tensile stress of pavement surface was not considered under the traffic load if GMTL were designed [21]. Since GMTL was prone to plastic deformation, the shear stress distribution law of the GMTL under 0.7 MPa load was studied, as shown in Figure 5.

Figure 5 shows that the maximum shear stress of the GMTL appeared at the $O_2$ point. Hence, the $O_2$ point was selected as the study point. The shear stress distribution of the $O_2$ point under different loads is shown in Figure 6. It can

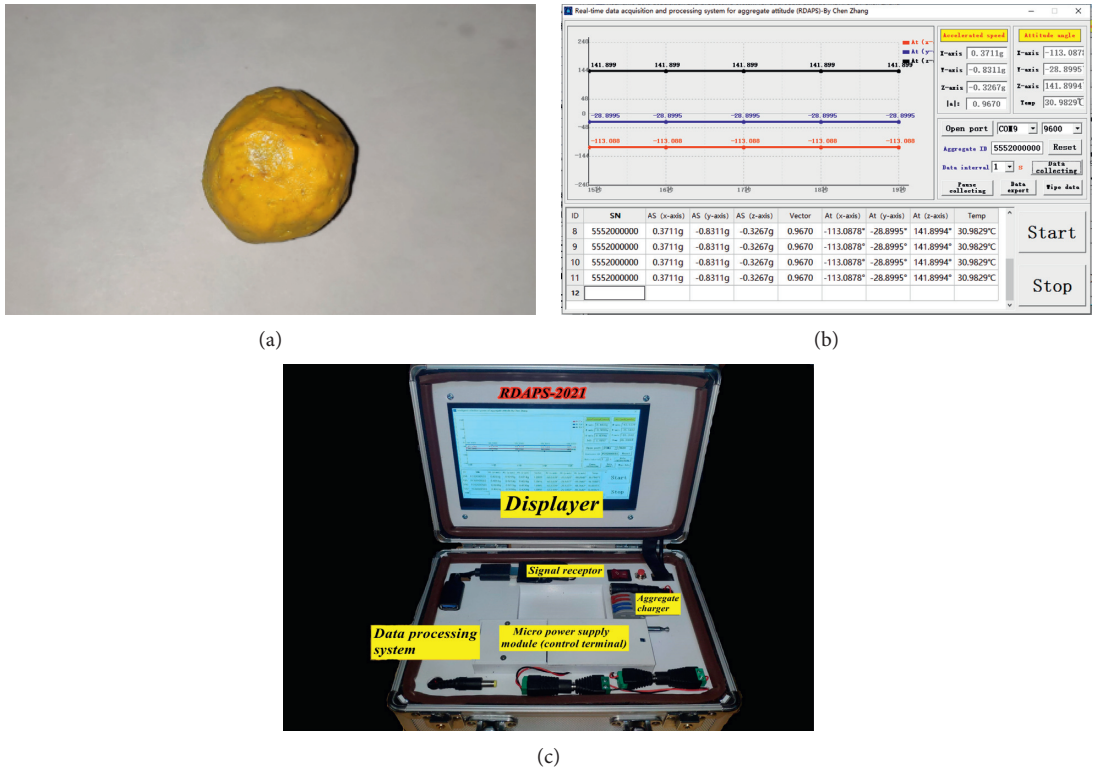


(a) (b) (c)

Figure 2: Introduction on RDAPS. (a) The appearance of WIAA. (b) Analysis software of RDAPS. (c) Hardware equipment of RDAPS.

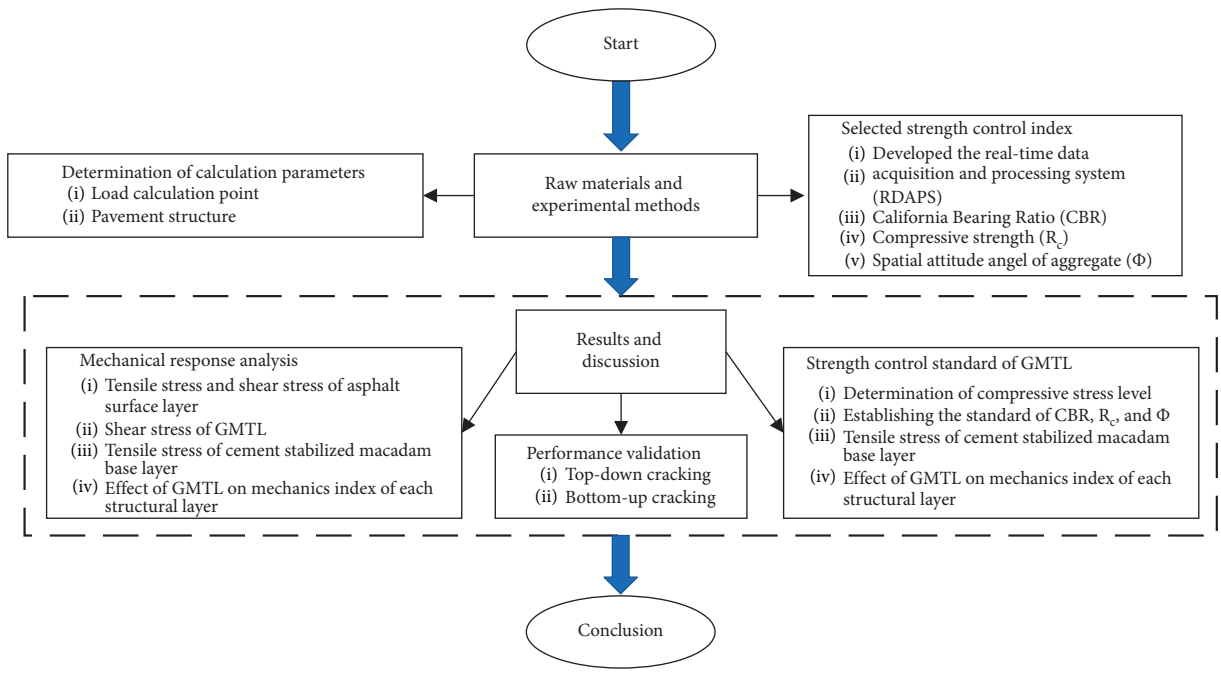


Figure 3: The research flow chart for this study.

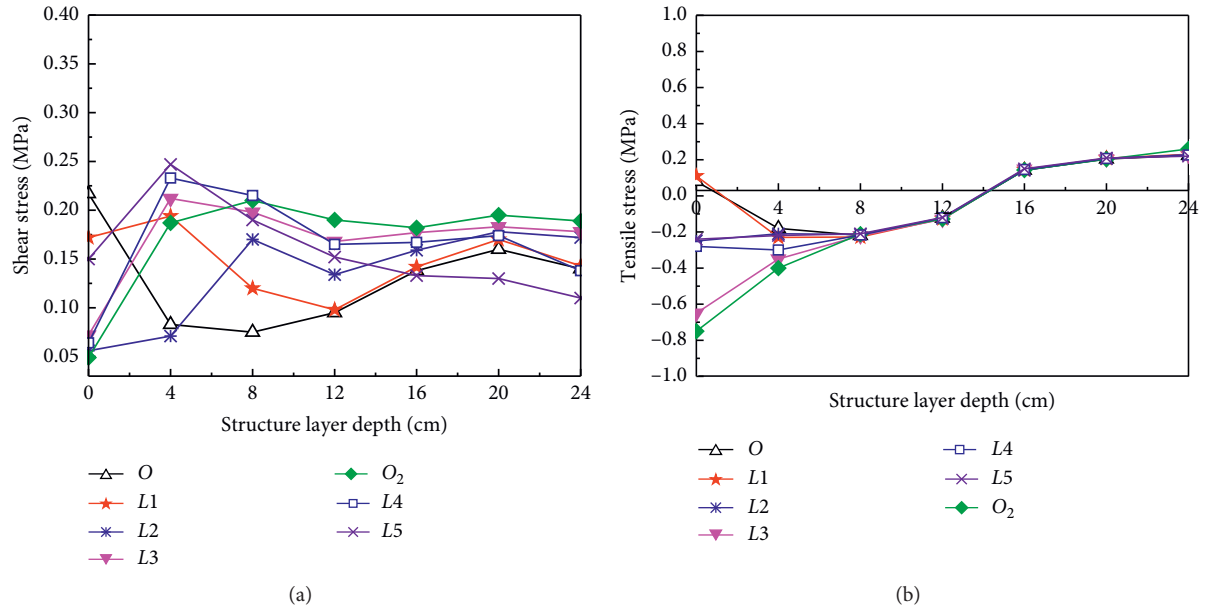


Figure 4: Stress distribution law of asphalt surface layer. (a) Shear stress distribution. (b) Tensile stress distribution.

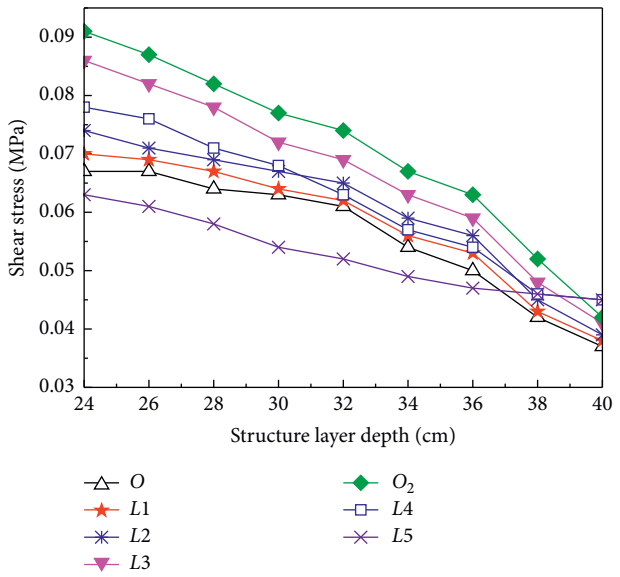


Figure 5: Shear stress distribution of GMTL.

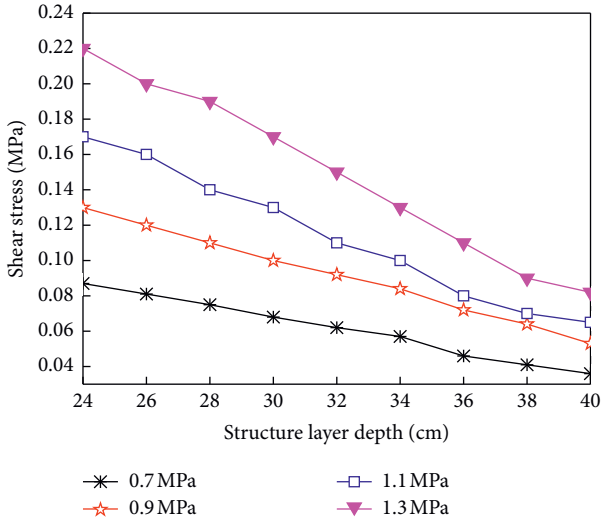


Figure 6: Influence of loading on distribution law of shear stress of $O_2$ point.

be seen from Figure 6 that the maximum shear stress of the GMTL increases linearly with an increase in load.

*3.1.3. Tensile Stress of Cement Stabilized Macadam Base Layer.* The tensile stress distribution law of cement stabilized macadam base layer under 0.7 MPa load is shown in Figure 7.

Figure 7 shows that the maximum tensile stress of the cement stabilized macadam base layer appears at the bottom of the *O* point, and the *O* point was selected as the research point of the tensile stress of the cement stabilized macadam base. The distribution law of base tensile stress at the *O* point under different loads is shown in Figure 8, which shows that the maximum tensile stress at the bottom of the cement stabilized macadam base layer increases linearly with an increase in load.

*3.1.4. Effect of GMTL on Mechanics Index of Each Structural Layers.* In order to facilitate calculation and analysis, the thickness range of GMTL is 12~20 cm and the modulus range is 300~800 MPa. The influences of the thickness and the modulus of GMTL on the tension stress at bottom of the surface layer, the maximum shear stress in GMTL, and the maximum tension stress in the semirigid base layer are shown in Figures 9–11.

According to Figure 9, when the modulus of GMTL varies from 300 MPa to 800 MPa, the maximum tensile stress

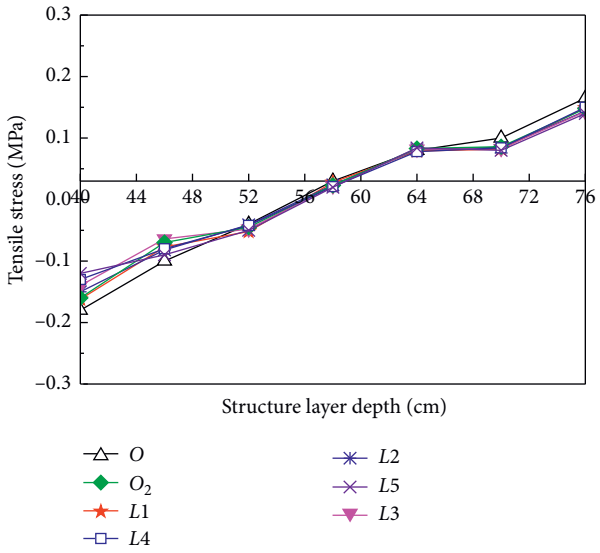


Figure 7: Tensile stress distribution of stabilized macadam base layer.

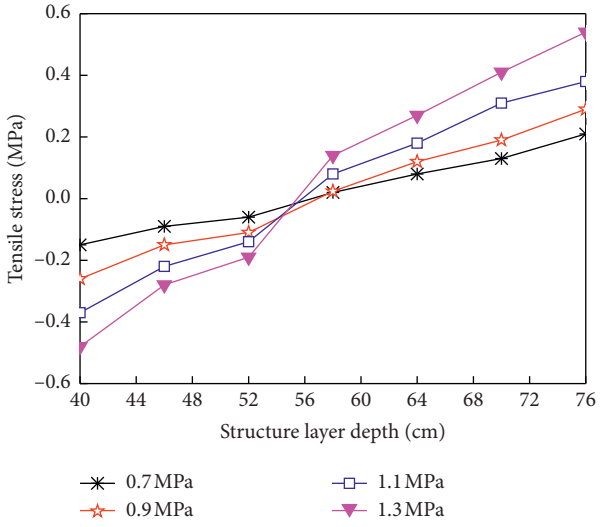


Figure 8: Tensile stress distribution of *O* cement stabilized macadam base layer point at different loading conditions.

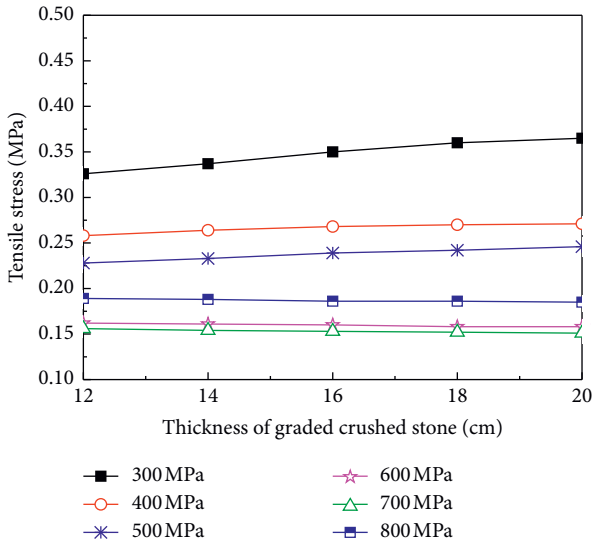


Figure 9: Influence on the maximum tensile stress at the bottom of the surface layer.

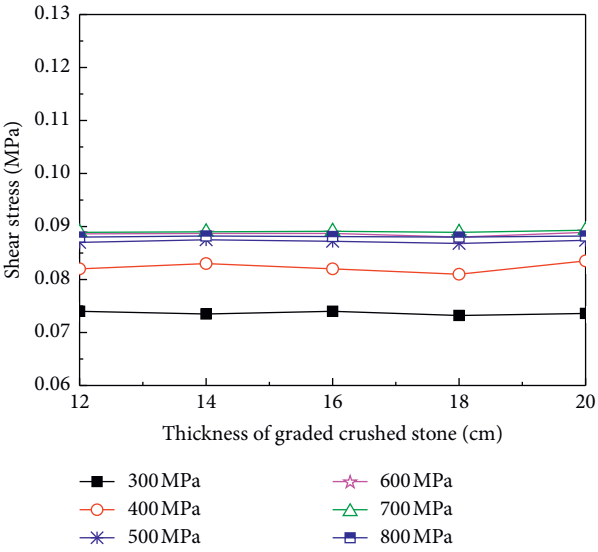


Figure 10: Influence on the maximum shear stress of GMTL.

at the bottom of the surface layer reduced by as high as 58%. When the thickness of GMTL is unchanged while the modulus is 700 MPa, the tension stress at the bottom of the surface layer was the smallest. When the modulus of GMTL was 300 MPa, the tensile stress at the bottom of the surface layer increased significantly. However, the increasing trend of the tensile stress got weakened with an increase in modulus. Figure 10 shows that when the thickness of GMTL is unchanged, the shear stress of GMTL increases as high 17% with an increase in modulus. When the thickness of GMTL is 18 cm, the self-shear stress is relatively minimum. Figure 11 shows that when the thickness of GMTL is constant, the change in modulus of GMTL has no significant effect on the tensile stress at bottom of the semirigid base layer. When the thickness of GMTL increases from 12 cm to 20 cm, the tensile stress at the bottom of the base layer reduced by about 31%.

It is concluded that the increase in modulus of GMTL can significantly reduce the tensile stress at the bottom of the surface layer and increase the shear stress in GMTL, but it has no significant effect on other stresses. The decrease in tension stress at the bottom of the semirigid base layer and increase in the tension stress at the bottom of the surface layer were observed with the increasing thickness of GMTL when the modulus of GMTL is set as 300 MPa. Based on the mechanics calculation results discussed above and the construction requirements in field, it is recommended that the optimum modulus and the thickness of GMTL are 700 MPa and 18 cm, respectively.

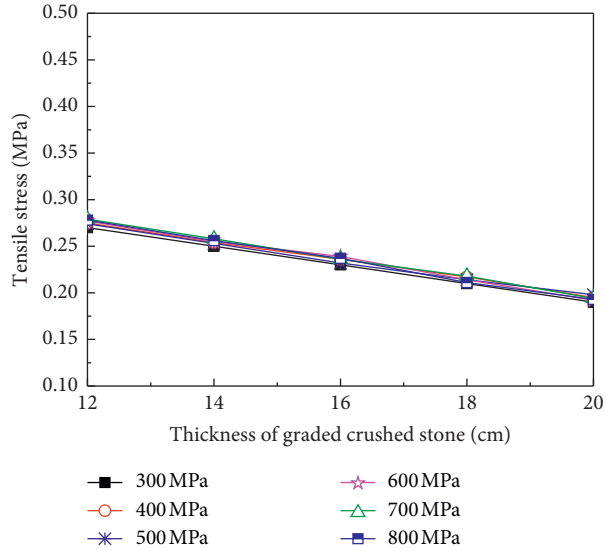


Figure 11: Influence on the maximum tensile stress in the semirigid base layer.

### 3.2. Strength Control Standard of GMTL

*3.2.1. Determination of Compressive Stress Level.* The information in Table 1 and the FIELD survey on the cumulative equivalent axle of heavy traffic road in the cold region chosen were used to calculate the compressive stress of the GMTL by means of the ABQUES. The results are shown in Table 2.

In this study, the mean value of 0.446 MPa was selected as the permitted compressive stress.

*3.2.2. Establishing the Strength Standard*

*(1) Compressive Strength Standard.* When the maximum compressive stress $\delta_{\max}$ exceeds the permitted value under the effect of vehicle load, permanent deformation will happen in GMTL [22]. Consequently, $\delta_{\max}$ should be less than the permitted compressive stress. According to the critical conditions, $R_c$ can be obtained if $\delta_{\max}$ is equal to the permitted compressive stress:

$$R_c = \delta_{\max} \times K_u, \tag{1}$$

where $K_u$ means the compressive strength coefficient.

According to the field investigation of the traffic volume and the "Specifications for Design of highway Asphalt pavement (JTG D50-2017)," the representative of the compressive strength coefficient under different traffic levels in the cold area of Hebei province was calculated. The result is shown in Table 3.

Taking the engineering situation in the field into consideration, the compressive strength coefficient of 2.37 is selected in this study. According to formula (1), the $R_c$ required for GMTL is 1.06 MPa under the level of heavy traffic in this area.

*(2) Standard of CBR.* $R_c$ can be turned into the CBR according to the relationship between CBR and $R_c$ [23]. In this study, the relationship between unconfined compression strength and CBR is shown in the following formula:

$$\mathrm{CBR} = \left(366R_c - 33.9\right) \times 100\%. \tag{2}$$

According to the previous formula, the CBR standard of GMTL is 354%. The CBR standard can better guide the design and construction of graded macadam materials subjected to the heavy traffic.

*(3) Strength Standard Based on the Spatial Attitude Angle of WIAA.* In this study, the mass ratio between coarse and fine aggregate is 69 to 31, and the void content is 10.3%. The WIAA was mixed into the aggregates. The heavy compaction test was conducted in one layer with compaction times of 150 under the optimum water content of 5.1%. The spatial attitude angle of WIAA was used to judge the interlocking condition of graded macadam. The calculation method of the spatial attitude angle is shown in the following formula:

$$\Phi = \sqrt{\Phi_x^2 + \Phi_y^2 + \Phi_z^2}, \tag{3}$$

where $\Phi$ is the spatial attitude angle and the unit is degree (°). $\Phi_x$ is the attitude angle in the $x$-axis direction. $\Phi_y$ is the attitude angle in the $y$-axis direction. $\Phi_z$ is the attitude angle in the $z$-axis direction. The strength standard of GMTL based on WIAA is determined according to the relationship between the spatial attitude angle of WIAA and the compaction degree of GMTL (see Figure 12).

As presented in Figure 12, with an increase in compaction times, $\Phi$ of WIAA showed a steep decreasing trend at the initial stage (less than 75 times), a stable decreasing trend at the middle stage (76~110 times), and a stable state at the third stage (111~150 times). This is because the initial stage of compaction is the transition stage of graded macadam from a loose state to a dense state, which causes $\Phi$ to decrease sharply [24]. At the middle stage of compaction, the graded macadam was further compacted, and the

Table 2: The compressive stress level of GMTL.

| Number of axle-load $N$ ($\times 10^6$) | Compressive stress of GMTL (MPa) | Mean values of compressive stress level (MPa) |
|---|---|---|
| 30 | 0.478 | |
| 40 | 0.439 | 0.446 |
| 50 | 0.421 | |

Table 3: The representative value of compressive strength coefficient in the Hebei cold region.

| Traffic level | Highway grade coefficient | Cumulative equivalent single axle loads | Compressive strength coefficient $K_u$ |
|---|---|---|---|
| Light traffic | 1.1 | $2\times10^6$~$15\times10^6$ | 1.92 |
| Medium traffic | 1.1 | $15\times10^6$~$30\times10^6$ | 2.14 |
| Heavy traffic | 1.0 | $30\times10^6$~$50\times10^6$ | 2.37 |

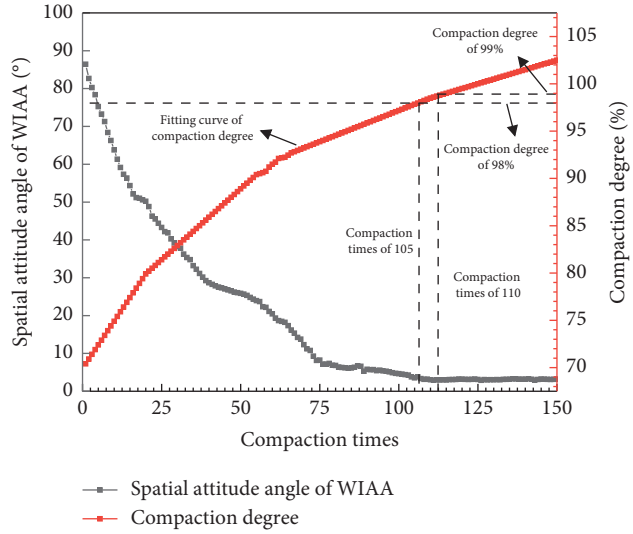


Figure 12: The relationship between spatial attitude angle and compaction degree.

interlocking skeleton between aggregates was formed at this stage. At this time, the movable space of WIAA is limited, and Φ decreases slowly. At the third stage of compaction, the interlock structure between aggregates in graded macadam had been in a fixed state. At this time, Φ of WIAA is stable at about 0.05 g/cm$^3$ due to the common drift phenomenon of sensors. When the compaction degree reaches 98% of the specification requirements, the corresponding compaction times are 105, and the spatial attitude angle of WIAA is not in a stable state at this time. Therefore, it is inferred that when the compaction degree of the graded macadam meets the requirements, there is still space for further optimization of the interlocking or contact state between the internal aggregates [25]. Taking this experiment as an example, the compaction degree was 99% at the 110$^{th}$ compaction while Φ of WIAA did not change anymore. Therefore, it is inferred that the interlock state between aggregates may be a relatively optimal state in terms of strength and stability. Based on the above analysis, it is concluded that Φ is a better indicator to characterize the strength and stability of GMTL in comparison to compaction degree.

According to Φ of WIAA, $R_c$ standard, and CBR standard discussed above, the strength control standard of IAP with GMTL is proposed, as shown in the following formula:

$$\begin{cases} \text{CBR} \geq 354\%, \\ Rc \geq 1.06\,\text{MPa}, \\ \phi_N \leq 3^\circ, \end{cases} \tag{4}$$

where $\Phi_N$ means the stable value of spatial attitude angle of WIAA after $N$ times compaction. The value of $N$ is determined by the actual situation. The three conditions in

Table 4: The optimized structure parameters of IAP.

| Layer | Material type | Thickness (cm) | Modulus (MPa) | Poisson ratio | Strength control standard |
|---|---|---|---|---|---|
| Top-surface | SMA-13 asphalt mastic crushed stone | 6 | 1450 | 0.25 | See formula (4) |
| Middle-surface | AC-20 asphalt mixture | 8 | 1600 | 0.25 | |
| Bottom-surface | AC-25 asphalt mixture | 9 | 1850 | 0.25 | |
| Top-base | Graded macadam transitional layer | 18 | 700 | 0.35 | |
| Bottom-base | Cement stabilized crushed stone | 36 | 8500 | 0.25 | |
| | Subgrade | | 40 | 0.40 | |

Table 5: Calculation parameters of Pavement-Me.

| Parameter type | Input level | Corresponding value |
|---|---|---|
| Service life | Level 2 | 20 years |
| Pavement structure | | See Table 4 |
| Material parameters | Level 2 and Level 3 | Dynamic modulus data of surface layer from laboratory test and the material parameters of based layer used the specification value |
| Traffic parameters | Level 3 | Heavy traffic |
| Climate parameters | Level 2 | Include temperature, rainfall, radiation, and humidity, which are from field survey and "National Meteorological Information Center" |
| Correction factor | | Default value be used, that is $\beta = 1.0$ |

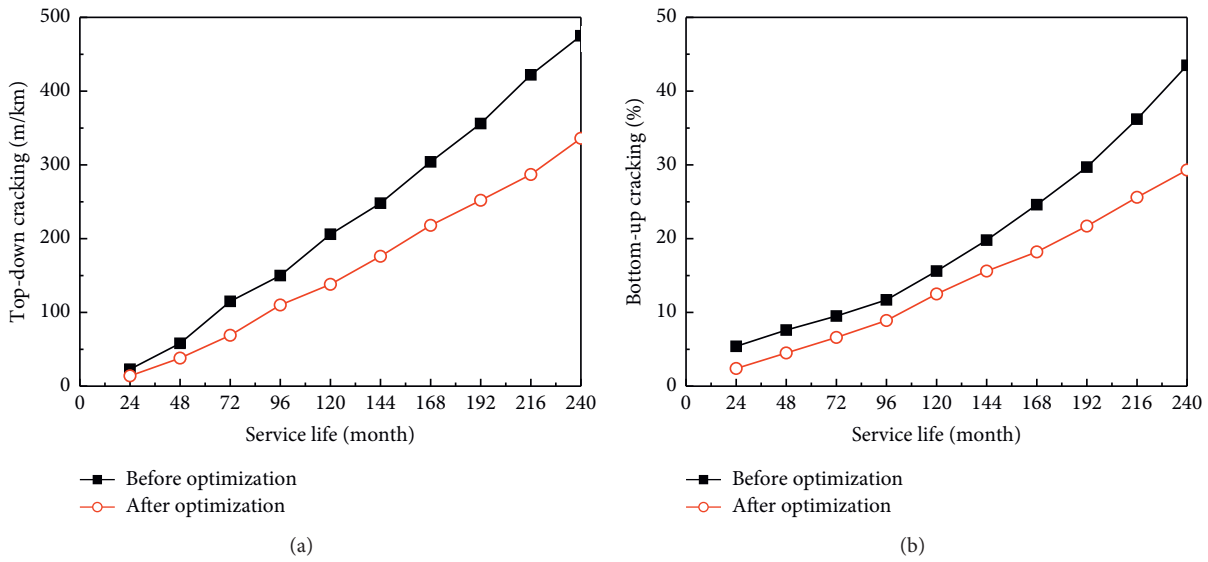


Figure 13: Prediction results of crack resistance based on Pavement-Me. (a) Top-down cracking. (b) Bottom-up cracking.

formula (4) must be reached at the same time. The final optimized pavement construction and parameters are shown in Table 4.

*3.3. Performance Validation by Pavement-Me Software.* According to the field survey, the main pavement distresses are top-down cracking and bottom-up cracking. The two types of cracking can be calculated using Pavement-Me software with the parameterized input level of Level 2 and Level 3. Pavement structure parameters are mentioned in Table 4. The parameter of material is expressed by dynamic modulus. The traffic parameter is the heavy traffic grade. The climate data can be obtained from the field survey and the meteorological data. The research in this part is designed to conduct a performance comparison. Hence, the default value is used for the correction factor of the MEPDG method [26]. The specific parameter is shown in Table 5.

The calculation results of Pavement-Me are shown in Figure 13.

From Figure 13, the top-down cracking of optimized pavement has been reduced by about 29.3% for the 20 years' service. For the bottom-up cracking, the bottom-up cracking of optimized pavement has been reduced by about 32.6% [27]. It is concluded that the asphalt pavement structure with GMTL has good resistance to cracking, which is consistent with the previous studies [28]. These findings can guide the construction and design of IAP in cold areas.

## 4. Conclusion

(1) With the increase in modulus of GMTL, the deformation in the surface layer would get less under a certain load, which makes the tension stress decreased. However, the force direction of the $O$ point chosen in this study had a trend to horizon direction from the vertical direction as long as the modulus of GMTL reached or closed to that of the asphalt mixture layer. The tensile stress at the bottom of the surface layer reduced up to 58% and the shear stress in GMTL increased up to 17% when the modulus of GMTL increases from 300 MPa to 800 MPa. The change in modulus has no significant influence on the maximum shear stress in the asphalt surface layer and the tensile stress in the base layer bottom.

(2) When the thickness of GMTL increases from 12 cm to 20 cm, the tensile stress in the bottom of the base layer reduced by about 31%. Combining the mechanical calculation results with the field technical requirements, the recommended optimal parameters of GMTL are the modulus of 700 MPa and the thickness of 18 cm.

(3) The spatial attitude angle $\Phi_N$ of wireless intelligent attitude aggregate (WIAA), the compressive strength $R_c$ standard, and the CBR standard were analyzed, and the strength control standard of inverted asphalt pavement with GMTL was proposed, that is, CBR $\geq$ 354%, $R_c \geq 1.06$ MPa, and $\Phi_N \leq 3^\circ$.

(4) In the cold region of Hebei, China, the optimized inverted asphalt pavement structure has a significant improvement in crack resistance. Taking the 20-year service life as an example, the damage degree of top-down cracks reduced by 29.3% and that of the bottom-up cracks reduced by 32.6% in comparison to the original structure.

## Data Availability

The data presented in this study are available on request from the corresponding author. The data are not publicly available due to privacy.

## Conflicts of Interest

The authors declare no conflicts of interest.

## Authors' Contributions

Y. L. performed investigation. C. Z. developed the methodology. C. Z. provided the software. Y. L. performed validation. All authors have read and agreed to the published version of the manuscript.

## Acknowledgments

This research was funded by the China Postdoctoral Science Foundation (2020M683402), Open Fund of Key Laboratory for Special Area Highway Engineering of Ministry of Education (Chang'an University) (300102210504), and the Science and Technology Planning Project of Xi'an (2020KJRC0046).

## References

[1] M. M. Karimi, N. Tabatabaee, H. Jahanbakhsh, and B. Jahangiri, "Development of a stress-mode sensitive viscoelastic constitutive relationship for asphalt concrete: experimental and numerical modeling," *Mechanics of Time-dependent Materials*, vol. 21, no. 3, pp. 383–417, 2017.

[2] L. Wang, Y. Hou, L. Zhang, and G. Liu, "A combined static-and-dynamics mechanics analysis on the bridge deck pavement," *Journal of Cleaner Production*, vol. 166, pp. 209–220, 2017.

[3] S. Lv, C. Liu, D. Chen, J. Zheng, Z. You, and L. You, "Normalization of fatigue characteristics for asphalt mixtures under different stress states," *Construction and Building Materials*, vol. 177, pp. 33–42, 2018.

[4] R. L. Lytton, Y. Zhang, F. Gu, and X. Luo, "Characteristics of damaged asphalt mixtures in tension and compression," *International Journal of Pavement Engineering*, vol. 19, no. 3, pp. 292–306, 2018.

[5] C. Si, E. Chen, Z. You, R. Zhang, P. Qiao, and Y. Feng, "Dynamic response of temperature-seepage-stress coupling in asphalt pavement," *Construction and Building Materials*, vol. 211, pp. 824–836, 2019.

[6] R. Behnke, I. Wollny, F. Hartung, and M. Kaliske, "Thermo-mechanical finite element prediction of the structural long-term response of asphalt pavements subjected to periodic traffic load: tire-pavement interaction and rutting," *Computers & Structures*, vol. 218, pp. 9–31, 2019.

[7] O. C. Assogba, Y. Tan, X. Zhou, C. Zhang, and J. N. Anato, "Numerical investigation of the mechanical response of semi-rigid base asphalt pavement under traffic load and nonlinear temperature gradient effect," *Construction and Building Materials*, vol. 235, Article ID 117406, 2020.

[8] S. Xie, J. Yi, H. Wang, S.-H. Yang, M. Xu, and D. Feng, "Mechanical response analysis of transverse crack treatment of asphalt pavement based on DEM," *International Journal of Pavement Engineering*, pp. 1–21, 2020.

[9] F. Tang, T. Ma, Y. Guan, and Z. Zhang, "Parametric modeling and structure verification of asphalt pavement based on BIM-ABAQUS," *Automation in Construction*, vol. 111, Article ID 103066, 2020.

[10] C. Li, Z. Fan, S. Wu, Y. Li, Y. Gan, and A. Zhang, "Effect of carbon black nanoparticles from the pyrolysis of discarded tires on the performance of asphalt and its mixtures," *Applied Sciences*, vol. 8, no. 4, p. 624, 2018.

[11] H. Li, H. Jiang, W. Zhang et al., "Laboratory and field investigation of the feasibility of crumb rubber waste application to improve the flexibility of anti-rutting performance of asphalt pavement," *Materials*, vol. 11, no. 9, p. 1738, 2018.

[12] L. C. Chow, D. Mishra, and E. Tutumluer, "Framework for development of an improved unbound aggregate base rutting model for mechanistic-empirical pavement design," *Transportation Research Record: Journal of the Transportation Research Board*, vol. 2401, no. 1, pp. 11–21, 2014.

[13] C. Lima and L. Motta, "Study of permanent deformation and granulometric distribution of graded crushed stone pavement material," *Procedia Engineering*, vol. 143, pp. 854–861, 2016.

[14] Y. C. Guo, L. G. Wang, A. Q. Shen et al., "Dynamic analysis of graded crushed stone as base of asphalt pavement," *Journal of*

*Highway and Transportation Reaseach and Development*, vol. 33, no. 1, pp. 27–33, 2016.

[15] Z. Q. Han, A. M. Sha, L. Q. Hu, and Z. Li, "Reasonable thickness of asphalt layer in graded crushed stone base asphalt pavement," *Journal of Chang'an University (Natural Science Edition)*, vol. 38, no. 4, pp. 1–9, 2018.

[16] G. Xu, Z. Chen, X. Li et al., "Simple prediction model for plastic deformation of graded crushed stone base for flexible pavement," *Materials and Structures*, vol. 53, no. 2, pp. 1–16, 2020.

[17] S. Wu, H. Chen, J. Zhang, and Z. Zhang, "Effects of interlayer bonding conditions between semi-rigid base layer and asphalt layer on mechanical responses of asphalt pavement structure," *International Journal of Pavement Research and Technology*, vol. 10, no. 3, pp. 274–281, 2017.

[18] N. S. Duong, J. Blanc, P. Hornych, B. Bouveret, J. Carroget, and Y. Le feuvre, "Continuous strain monitoring of an instrumented pavement section," *International Journal of Pavement Engineering*, vol. 20, no. 12, pp. 1435–1450, 2019.

[19] Ministry of Transport of the People's Republic of China, *Specifications for Design of Highway Asphalt Pavement: JTD D50-2017*, China Communications Press, Beijing, China, 2017.

[20] J. Jin, S. Liu, Y. Gao et al., "Fabrication of cooling asphalt pavement by novel material and its thermodynamics model," *Construction and Building Materials*, vol. 272, no. 12, Article ID 121930, 2021.

[21] J. Peng, J. Zhang, J. Li, Y. Yao, and A. Zhang, "Modeling humidity and stress-dependent subgrade soils in flexible pavements," *Computers and Geotechnics*, vol. 120, Article ID 103413, 2020.

[22] P. Mackiewicz, "Finite-element analysis of stress concentration around dowel bars in jointed plain concrete pavement," *Journal of Transportation Engineering*, vol. 141, no. 6, Article ID 06015001, 2015.

[23] D. B. Eme, T. C. Nwofor, and S. Sule, "Correlation between the California bearing ratio (CBR) and unconfined compressive strength (UCS) of stabilized sand-cement of the niger delta," *International Journal of Civil Engineering*, vol. 3, no. 3, pp. 7–13, 2016.

[24] G. Qian, K. Hu, J. Li, X. Bai, and N. Li, "Compaction process tracking for asphalt mixture using discrete element method," *Construction and Building Materials*, vol. 235, Article ID 117478, 2020.

[25] G. D. Airey and A. C. Collop, "Mechanical and structural assessment of laboratory- and field-compacted asphalt mixtures," *International Journal of Pavement Engineering*, vol. 17, no. 1, pp. 50–63, 2016.

[26] K. Ng, D. Hellrung, K. Ksaibati, and S. S. Wulff, "Systematic back-calculation protocol and prediction of resilient modulus for MEPDG," *International Journal of Pavement Engineering*, vol. 19, no. 1, pp. 62–74, 2018.

[27] C. Liu, S. Lv, D. Jin, and F. Qu, "Laboratory investigation for the road performance of asphalt mixtures modified by rock asphalt-styrene butadiene rubber," *Journal of Materials in Civil Engineering*, vol. 33, no. 3, Article ID 04020504, 2021.

[28] C. Liu, S. Lv, X. Peng, J. Zheng, and M. Yu, "Analysis and comparison of different impacts of aging and loading frequency on fatigue characterization of asphalt concrete," *Journal of Materials in Civil Engineering*, vol. 32, no. 9, Article ID 4020240, 2020.